Wind and Structures, Vol. 16, No. 2 (2013) 179-192
DOI: http://dx.doi.org/10.12989/was.2013.16.2.179

Flow-pattern identification around two rectangular cylinders with aspect ratio of 0.5 in tandem arrangement

Letian Yang*[1,2], Zhifu Gu[2] , Xuejun Zhao[1] and Weimin Zhang[1]

[1]*China Academy of Aerospace Aerodynamics, Beijing, China, 100074*
[2]*LTCS and College of Engineering, Peking University, Beijing, China, 100871*

(Received October 16, 2009, Revised February 11, 2011, Accepted January 10, 2012)

Abstract. The flow around two rectangular cylinders with aspect ratio of 0.5 in a tandem arrangement, was investigated using pressure measurements (in a wind tunnel) and flow visualizations (in a water tunnel) in the range of P/h from 0.6 to 4.0. Four flow patterns were identified, and processes of shear layers wrapping around, the shear layer reattachment, vortices wrapping around and vortices impingement, were observed. Mean and rms pressure distributions, flow visualizations and Strouhal numbers were presented and discussed. The paper revealed that the variations of Strouhal numbers were associated with the shear layers or vortex interference around two cylinders.

Keywords: rectangular cylinders; pressure distributions; flow visualizations; flow patterns

1. Introduction

Because of its common occurrence in many forms and different applications (e.g., bridges, buildings and offshore facilities), flows around rectangular cylinders were studied by many researchers in the last few years. A large amount of knowledge has been accumulated for the characteristics of the isolated rectangular cylinder (i.e., the Strouhal numbers, the pressure distributions and the shear layer development, etc) has been obtained by experimental and numerical investigations (Courchesne and Laneville 1979, Laneville and Lu 1983, Noda and Nakayama 2003, Nakaguchi *et al*. 1968, Okajima 1982, Norberg 1993, Sohankar 2008, Yu and Kareem 1997, Oka and Ishihara 2009, Lim 2009)

It is well known, however, the characteristics of wind loading on members in a group may be quite different from that on the isolated one due to the interference of each other and some interesting and unexpected phenomenon will be exhibited. As the simplest case of a group of structures, two rectangular cylinders in a tandem arrangement are often found in practice and numerous investigations have been performed on, particularly for the cases with cylinders with aspect ratio of 1. Bailey (1985) studied two tall square buildings in a low-turbulence wind environment and got the conclusion that the dynamic loads on the upstream building might increase by a factor of up to 4.4, and on the downstream one might increase by a factor of up to 3.2. Possible excitation mechanisms were discussed and critical building arrangements were presented.

*Corresponding author, E-mail: ylt@pku.edu.cn

Xie and Gu (2005) studied the static and dynamic interference effects on a high-rise prismatic structure due to the excitation of several types of upwind structures with various breadths and heights in different upwind terrains. The results showed that the interfering structure of smaller breadth could lead to a vortex-induced resonance at the lower reduced velocity and cause pronounced effects on the interfered structure. Zhang and Gu (2008) presented numerical and experimental investigations of the wind-induced interference effects on two square buildings in staggered arrangements. Specifically, the mean pressure, fluctuating pressure and moment measurements on the principal building with interference from surroundings at different wind directions were obtained. Sakamoto *et al*. (1987) observed significant changes in the time-mean and fluctuating forces acting on the two tandem square cylinders for spacing ratios L/D<4.0 and L/D>4.0 at Re=2.76×10^4 and 5.52×10^4. The changes were associated with two different flow patterns: the suppression of the regular vortex shedding from the upstream cylinder for L/D<4.0 and the beginning of the periodical vortex shedding from each cylinder for L/D=4.0. At the critical spacing ratio L/D=4.0, the time-mean drag and fluctuating lift and drag on the two cylinders were found to jump discontinuously and reach the maximum values. Luo and Teng (1990) and Luo *et al*. (1999) also found similar results at Re=5.67×10^4. Sakamoto and Haniu (1988) further investigated the characteristics of the time-mean and fluctuating forces acting on two square prisms placed vertically in various arrangements in a turbulence boundary layer. According to the variation of the Strouhal number with the spacing between the two prisms, two regions (called 'Reattachment' and 'Synchronized vortex shedding') were classified in the case of the tandem arrangement. However, this classification was somewhat not extensive and few attentions were paid on the development of the shedding vortex and the interactions between the two cylinders. Liu (2002) reported an experimental study on the flow characteristics around two square cylinders in a tandem arrangement at Reynolds number ranging from 2.0×10^3 to 1.6×10^4. The hysteresis with two discontinuous jumps was observed at all Reynolds number, which was associated with two different flow patterns: Mode I and Mode II. In the hysteresis regime, the drag coefficients as well as the fluctuating pressures of the two cylinders corresponding to the flow pattern of Mode I generally showed at a discernibly lower level than those corresponding to the flow pattern of Mode II. The extent of the jump in drag coefficient for the downstream cylinder appeared to be several times larger than that for the upstream cylinder. Kim *et al*. (2008) investigated the velocities, turbulence intensities, Reynolds shear stresses and turbulent kinetic energies of the flow fields around two tandem square cylinders with particle image velocimetry (PIV) method at Re=5.3×10^3 and 1.6×10^4. The results showed that the flow pattern at s/D≤2.0 was drastically different from that at s/D≥2.5 for both Reynolds numbers. The sudden change of the flow patterns depended on the reattachment of the shear layer separated from the upstream cylinder.

Compared with the square cylinders, systematic investigations for rectangular cylinders are few. Sun et al. [20] did experiments on the two staggered rectangular cylinders with different aspect ratio (0.3-5.0), in addition to different pitch ratio (0.3-8.0) and incidence angle (0°-90°) in the uniform smooth flow at Re=1.03×10^5. The pressure distributions, drag coefficients C_D, lift coefficients C_L of the two cylinders were provided. A 'jump' phenomenon of the C_D on the rear cylinder was observed in the tandem case, when the C_D jumped from negative to positive from L/h=4.1 to L/h=4.2. However, no comprehensive explanation of this phenomenon was given.

This paper aims to investigate experimentally the flow patterns around two rectangular cylinders with aspect ratio of 0.5 in a tandem arrangement. Mean and rms pressure distributions were conducted in a wind tunnel. Flow visualizations were conducted in a water tunnel. Four flow

patterns, processes of shear layers wrapping around, the shear layer reattachment, vortices wrapping around and vortices impingement, were classified and discussed. The variations of Strouhal numbers were also discussed at different flow patterns. Moreover, for a better understanding of the mechanism for the interference, comparisons with the flow patters of two circular cylinders in the tandem arrangement studied by Sumner *et al*. (2005), Sumner *et al*. (2000), Zhou and Hu (2008) are also given.

2. Experimental approach

In this paper, pressure measurements and flow visualizations were conducted to obtain pressure distributions, St number and flow visualization pictures. The pressure measurement and flow visualizations were conducted in a uniform smooth flow with Reynolds number $Re=5\times10^4$ at a wind tunnel and with Reynolds number Re=2100 at a water tunnel, respectively. Two different setups were used for the difference size of the wind tunnel and the water tunnel.

2.1 Pressure measurements

The experiments were conducted in a low-speed, closed-returned wind tunnel at Peking University. The tunnel has an open circular test section 2.25 m in diameter and 3.65 m long. Under uniform smooth flow condition, the background turbulence intensity in the test place is 0.6%.

The experimental set-up is showed in Fig. 1(a). Both of the models were 600 mm long (designated as L). The cylinders, with circular end plates of 500 mm diameter at both ends, were mounted perpendicularly in one adjustable guide-slot which made the adjustment of the pitch ratio (designated as P/h) of the cylinders easy. The lower end plate was positioned 250 mm away from the test-section floor of the tunnel so that the cylinders were located outside the boundary layers developing on the floor.

Fig. 1(b) is a schematic diagram showing the arrangement of the two parallel rectangular cylinders. Both of the cylinders were 50mm high (designated as h), 25 mm width (designated as b), with the aspect ratio b/h=0.5. P/h was the pitch ratio between the two cylinders, where P was the distance between the centers of two cylinders. Both of the cylinders were arranged with 50 mm side (the height side) normal to the incident flow. The range of the pitch ratio P/h was from 0.6 to 4.0 with a necessary increment. The blockage was about 2.2%. Pressure taps (u1-u16 on the upstream cylinder and d1-d16 on the downstream cylinder) were installed equidistantly around the cylinders at the mid-span, with five taps on the front (or back) surface and three taps on each of the side surface.

The measurement system for the surface pressure consisted of pressure transducers (PDCR-23d), a set of Scanivalves (SGM-48), five DC amplifiers (6M72), an A/D converter and a personal computer with LabView (NI) software. The sampling frequency is 400 Hz. In order to obtain frequency response as high as possible, the plastic tubes with restrictors were used to connect the taps to Scanivalves. The frequency response of the system was measured such that: when the frequency below 125 Hz, the relative error of value of amplitude was less than 2% and phase delay might be ignored.

The Reynolds number Re is defined as Re=U×h/ν, where U is mean wind velocity of the oncoming flow, h is the height of the cylinders and ν is kinetic aerodynamic viscosity coefficient. In this study, the pressure measurement experiments were all conducted at $Re=5\times10^4$.

The mean and rms pressure coefficient C_p and C_{rms} is defined as $C_p=\frac{\overline{P}-P_0}{q}, C_{rms}=\frac{\sigma}{q}$, respectively, where $\overline{P}, P_0, \sigma$ and q are the mean pressure, the static pressure of oncoming flow, the rms pressure and the dynamic pressure on a reference height, respectively. The reference height is as high as the pressure taps. The positive pressure is defined as the pressure pointing inner to the cylinder's surface and the negative pressure is the suction pointing outside of the surface. The pressure distributions on the cylinders are present along A (A')-B (B')-C (C')-D (D')-A (A'), as shown in Fig. 1(b).

The mean drag coefficient, denoted by C_D, is defined conventionally and is obtained by integrating appropriately the mean pressure distributions.

The Strouhal number is defined with the frequency at which a pronounced peak occurs at the power spectral density of the fluctuating pressure. St=f×h/U, where f is the frequency as mentioned, U is mean wind velocity of the oncoming flow and h is the height of the cylinders, respectively. The peak strength is normalized by the square of the dynamic pressure at the reference height Noda and Nakayama (2003). In this paper, since the two cylinders were arranged symmetrically, the Strouhal numbers were only studied on five pressure taps: u7, u9, d5, d7 and d9, as shown in Fig. 1(b).

2.2 Flow visualizations

In order to explain some interesting phenomena appearing in the pressure measurements, the hydrogen bubble flow visualizations were conducted later in a closed-loop water tunnel at Re=2100, with a 500mm×500mm cross-section working section, and a free-stream turbulence intensity of 0.03%. Two identical rectangular cylinders with h=30 mm and b=15 mm were mounted perpendicularly with respect to the mid-plane of the working section. The gap between the cylinder end and the tunnel base was about 3 mm. The cylinder blockage was 6%, and the slenderness ratio exceeded 16. The arrangements conducted here were the same with the pressure measurements.

The power source for the hydrogen bubble generator consisted of an autotransformer, which ranged between DC 0-30 volts. The pulse generator was a periodical switch circuit and had different frequencies which could be changed consecutively.

Hydrogen bubble platinum wires with a diameter of 0.6 mm were used in this study. Two or three wires were used, with respect to the resolution of the flow structure around the cylinders. The wires were placed parallel to the height side of the cylinders with 500 mm away from the sides and fixed to two 2 mm-thick sheets, which were affixed on the two walls of the tunnel. The wires were tensioned and connected to the cathode of the hydrogen bubble generator. The anode was made up of the graphite, which was downstream and far away enough from the working section.

The hydrogen bubble wires were illuminated by a light source, located on one side of the water tunnel. A light sheet was set up when the light passed through a slit. The thickness of the light sheet and a suitable brightness could be achieved by adjusting the width of the slit. The illuminated flows were recorded by a SONY video camera recorder DSR-PD190P which could provide a high-quality image, and the still pictures were captured by the media recorder.

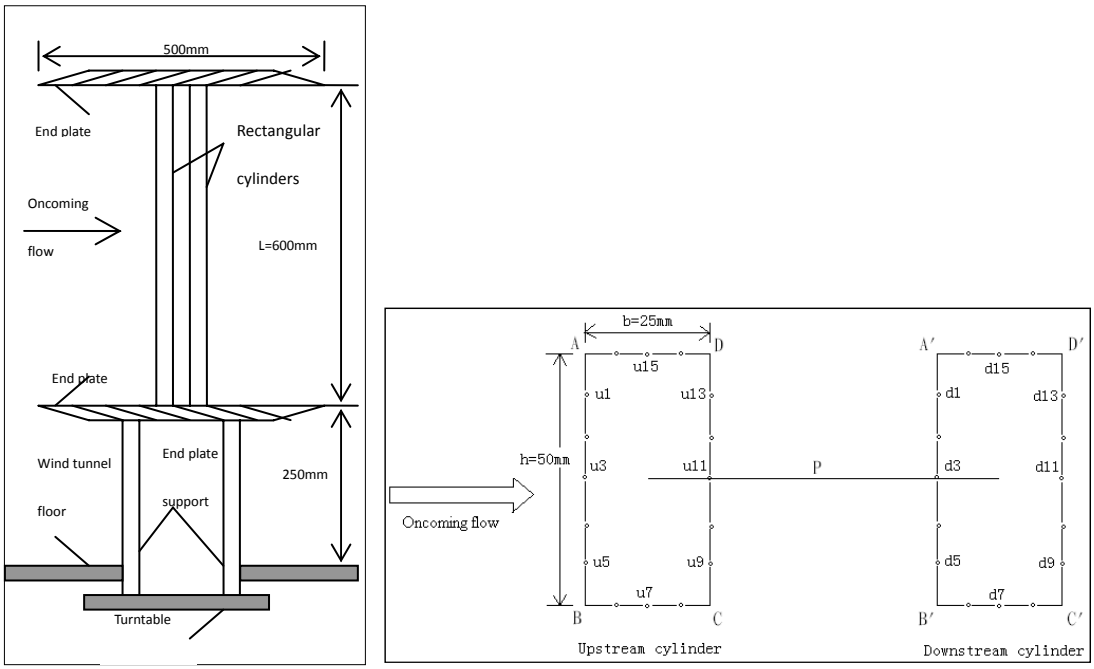

(a) (b)

Fig. 1 Schematic diagram: (a) The set-up in wind tunnel and (b) Arrangement of the two-cylinder.

3. Results and discussion

3.1 The isolated rectangular cylinder

In order to perceive the effect of the group interference, the result for the isolated cylinder was measured first, and then compared with that of the cylinders in the tandem arrangement. Fig. 2(a) shows the mean pressure distributions along four surfaces of the cylinder. The pressure distributions on the front surface C_{pf} are symmetric. The pressure distributions on the side surface C_{ps} and the back surface C_{pb} are almost uniform and equal to 1.39 and 1.45, respectively, which are quite similar with others literatures, including experimental data (Courchesne and Laneville 1979, Norberg 1993, Lim 2009) and numerical simulation data (Sohankar 2008, Yu and Kareem 1997, Oka and Ishihara 2009), Fig. 2(b) shows the rms pressure distributions along the cylinder. The C_{rms} on the front surface are quite small, attributing to the small fluctuation of the oncoming flow. However, on the side and back surfaces, the C_{rms} are quite large, due to the strong alternate shedding of the shear layers. The power spectral density of the fluctuating pressure on the side surfaces is represented in Fig. 2(c). Only one prominent peak exists at St=0.12, which is also quite similar with the literatures (Courchesne and Laneville 1979, Nakaguchi *et al*. 1968). Peaks are seen on all surfaces except near the center of the front surface. Further more, 2St is detected on the center of the back surface, as shown in Fig. 2(d), which is attributing to the regular alternate shedding of the vortices.

Since the experimental conditions, such as turbulence intensity, aspect ratio, blockage and

Reynolds number, are different, there are some difference between present data and the previous test data (Courchesne and Laneville 1979, Nakaguchi *et al*. 1968, Norberg 1993, Lim 2009).

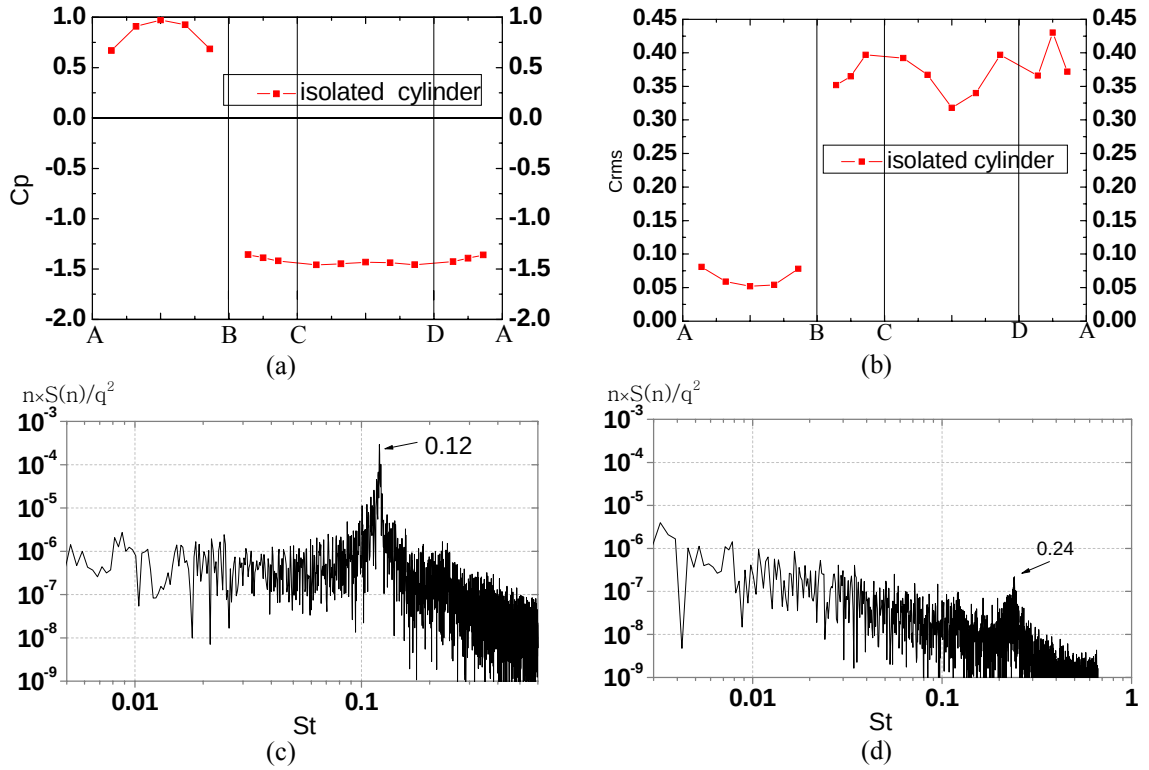

Fig. 2 Results for the isolated cylinder: (a) Mean pressure distributions, (b) Rms pressure distributions, (c) Power spectral density on the side surfaces and (d) Power spectral density on the center of the back surface

3.2 Classifications for pressure distributions

Figs. 3(a), (c) and (d) show the mean pressure distributions C_p and rms pressure distributions C_{rms} along both rectangular cylinders with five typical pitch ratios (P/h=0.6, 2.0, 3.6, 3.7, 4.0), respectively. In order to obtain a more understanding for the mean pressure distributions C_p, the variations of C_D on the two cylinders are shown in Fig. 3(b). From Fig. 3(a) it can be seen that the C_{pf} of the upstream cylinder are symmetric and almost the same at all pitch ratios. At P/h=0.6-3.6, the C_{pf} of the downstream cylinder are almost uniform and equal to the C_{pb} of the upstream cylinder, which suggests that the flow within the gap is somewhat 'stagnant'. From Fig. 3(b) it can be seen that at P/h=0.6-3.6, the C_D of the upstream cylinder decreases gradually. Meanwhile, the C_D of the downstream cylinder also changes gradually and keeps negative. From Fig. 3(c) it can be seen that the C_{rms} on the front surface of the upstream cylinder are quite small (lower than 0.1) at

all pitch ratios, which is caused by the small fluctuation of the oncoming flow.

At P/h=0.6, the C_{ps} and C_{pb} of the downstream cylinder are small and quite similar with that of the isolated one, as mentioned in Fig. 2(a). Meanwhile, the C_{ps} on the two cylinders are quite uniform and almost the same with each other, which suggests that no shear layer reattaches on the side surfaces. In this configuration, the C_D of the upstream cylinder has a maximum value, due to the minimum C_{pb}. On the other hand, the C_{rms} on the front surface of the downstream cylinder are quite large and almost equal to that on the back surface of the upstream cylinder. Further more, the C_{rms} on the side and back surfaces of the downstream cylinder are large too and quite similar with that of the isolated one, as mentioned in Fig. 2(b). This type of pressure distributions will be denoted by 'shear layers wrapping around pattern (SLWA)' for further reference.

As P/h increases to 2.0, the C_p on the two cylinders (except the C_{pf} of the upstream cylinder) increase, resulting in a smaller C_D on the upstream cylinder. Meanwhile, the C_{ps} of the downstream cylinder rise from B' to C' (or A' to D'), which indicates that the shear layers separated from the upstream cylinder tend to be close to the side surfaces of the downstream cylinder. On the other hand, compared with P/h=0.6, the C_{rms} on the two cylinders are much smaller, especially on the upstream cylinder. For the downstream cylinder, the C_{rms} on the side surface are larger than that on other parts, suggesting that the flow around the side surfaces is more fluctuant. This type of pressure distributions will be denoted by 'the shear layer reattachment pattern (SLR)' for further reference.

When P/h=3.6, the C_p on the two cylinders (except the C_{pf} of the upstream cylinder) still increase, resulting in a smaller C_D on the upstream cylinder again. Since the C_{pf} of the downstream cylinder are almost equal to C_{pb}, the C_D on the downstream cylinder equals to about 0. Meanwhile, the C_{ps} of the downstream cylinder keep uniform. On the other hand, the C_{rms} on the side and back surfaces of the two cylinders are slightly larger than that at P/h=2.0, but the C_{rms} on the front surface of the downstream cylinder are much larger than that at P/h=2.0, which means that the flow around there becomes more fluctuant. This type of pressure distributions will be denoted by 'vortexes wrapping around pattern (VWA)' for further reference.

An interesting phenomenon happens at P/h=3.7, where the C_{pf} of the downstream cylinder abruptly increase, meanwhile, the C_{ps} and C_{pb} drop a little. This phenomenon results in a C_D 'jump', where the C_D of the downstream cylinder jumps from a negative value (C_D=-0.07 at P/h=3.6) to a positive value (C_D=0.32 at P/h=3.7), as shown in Fig. 3(b). Sun and Gu (1995) also observed the C_D of the rear rectangular cylinder (b/h=0.5) jumped from negative to positive from L/h=4.1 to L/h=4.2 for the tandem case, but no explanation was given. The C_p of the two cylinders at P/h=4.0 are just the same with that at P/h=3.7, which are still quite different from that of the isolated one, meaning that the interference between the two cylinders still exists. On the other hand, the C_{rms} on the front surface of the downstream cylinder also increase abruptly and are even larger than that at P/h=0.6. This is corresponding to the C_D 'jump', as mentioned above. Meanwhile, the C_{rms} on the side and back surfaces of the two cylinders also become larger than that at P/h=3.6, but are still smaller than that at P/h=0.6. When P/h increases to 4.0, the C_{rms} on the downstream cylinder are similar with that at P/h=3.7. However, the C_{rms} on the upstream cylinders are still getting larger. This type of pressure distributions will be denoted by 'vortexes impingement pattern (VI)' for further reference.

3.3 Flow visualizations

In order to investigate the interesting phenomenon observed in the pressure distributions, the

flow visualizations were conducted with the hydrogen bubble technique at Re=2100. The results are present at P/h=0.6, 2.0, 3.6, 4.0, as shown in Fig. 4. In general, four remarkably different flow patterns are observed, corresponding to the four pressure distribution patterns mentioned in §3.2.

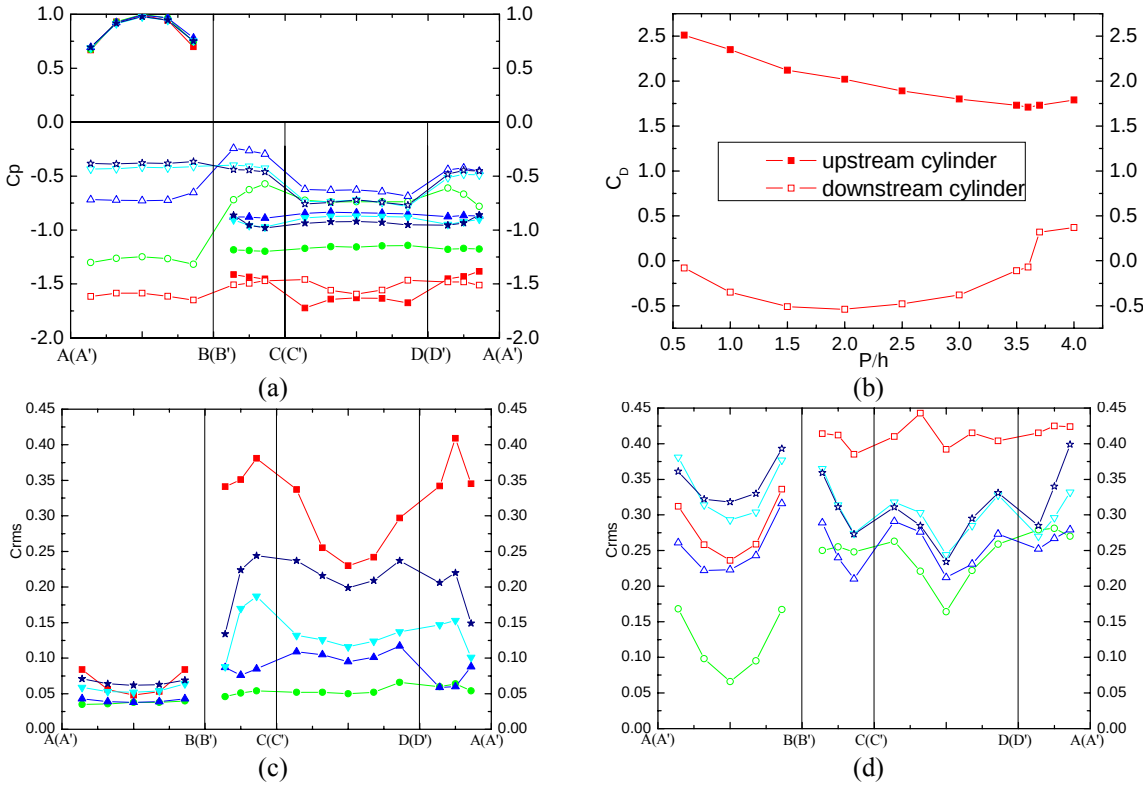

Fig. 3 The variations of: (a) Mean pressure distributions with P/h, (b) Mean drag coefficients with P/h; (c) Rms pressure distributions with P/h: upstream cylinder and (d) Rms pressure distributions with P/h: downstream cylinder

-■-: P/h=0.6, upstream cylinder; -□-: P/h=0.6, downstream cylinder; -●-: P/h=2.0, upstream cylinder; -○-: P/h=2.0, downstream cylinder; -▲-: P/h=3.6, upstream cylinder; -△-: P/h=3.6, downstream cylinder; -▼-:P/h=3.7, upstream cylinder; -▽-:P/h=3.7, downstream cylinder; -★-:P/h=4.0, upstream cylinder; -☆-:P/h=4.0, downstream cylinder.

The flow visualization pictures observed at P/h=0.6, as shown in Figs. 4(a) and (b), indicate clearly that the shear layers separate from the upstream cylinder alternately and warp around the whole downstream cylinder, which is denoted by shear layers wrapping around flow pattern (SLWA). The two cylinders seem like 'one-body', which can explain why the C_{ps} and C_{pb} of the downstream cylinder are quite similar with that of the isolated one. Meanwhile, the strong shedding of the shear layers also results in the large C_{rms} occurring on the two cylinders (except the front surface of the upstream cylinder), and further more, since the gap between the two cylinder is

small, the C_{rms} on the back surface of the upstream cylinder are almost equal to that on the front surface of the downstream cylinder, as mentioned in §3.2. A similar result is also observed by Sumner *et al*. (2005) (at the closely spaced staggered configurations at α=0°) and Hu amd Zhou (2008) (at mode S-Ⅰ).

When P/h=2.0, the flow visualization picture shown in Fig. 4(c) indicates that the shear layer from the upstream cylinder reattaches onto the sides of the downstream cylinder alternately and rolls up into its rear, which was also observed by Sumner *et al*. (2005) at the moderately spaced staggered configurations at α=0°. This pattern is denoted by the shear layer reattachment flow pattern (SLR). No shear layer rolls up into the gap region, resulting in the 'stagnant' phenomenon, as discussed in §3.2. Meanwhile, for the downstream cylinder, this reattachment on the side may be the reason why the C_{ps} rise from B' to C' (or A' to D'), and the C_{rms} on the side surface (or the outer-part of the front and back surfaces) are much larger than that on other parts. On the other hand, from the flow visualization video, it can be seen that since the shear layer reattaches onto the side surface, the shedding strength of the shear layers is weaker than that at P/h=0.6, which results in a smaller C_{rms} on the two cylinders.

A change happens at P/h=3.6, as shown in Fig. 4(d), indicating clearly that the vortices shedding from the two sides of the upstream cylinder wrap around the downstream cylinder and result in a 'stagnant' phenomenon again on the gap region, which is corresponding to Fig. 3(a). This pattern is denoted by vortices wrapping around flow pattern (VWA). No shear layer reattachment occurs on the side surfaces of the downstream cylinder. Since vortices are separated from the upstream cylinder and formed around the downstream cylinder, the C_{rms} on the two cylinders, especially on the front surface of the downstream cylinder, are larger than that at P/h=2.0. Two rows of vortex streets are observed behind the upstream cylinder.

From the pressure distributions, it is evident that the configurations of P/h=3.7-4.0 belong to the same pattern. The flow visualization picture at P/h=4.0, representing the vortices impingement flow pattern (VI), is shown in Fig. 4(e). It indicates clearly that in this pattern the vortex shedding from one side of the upstream cylinder impinges upon the front surface of the downstream cylinder. This 'impingement' will results in an abrupt increase of C_p and C_{rms} on the front surface of the downstream cylinder, and a 'jump' of C_D, as mentioned in §3.2. On the other hand, compared with P/h=3.6, the gap between the two cylinders is larger, resulting in a more complete development of the shear layers from the two cylinders and, a larger C_{rms} on the two cylinders, as mentioned in §3.2.

The schematic representations of different flow patterns based on the flow visualization video are shown in Figs. 5(a) - (d).

3.4 Variations of Strouhal numbers

The variations of Strouhal numbers with the change of P/h are present in Table 1. Since the two cylinders are arranged symmetrically, the St is only studied on u7, u9, d5, d7 and d9 taps. Meanwhile, the power spectral density on u9 and d9 with the change of P/h are shown in Figs. 6 and 7, respectively, as the typical examples.

In this section, the characteristics of St in each pattern are discussed based on the flow visualizations. Further more, according to the pressure distributions and St number, the boundaries for the four flow patterns are proposed: the SLWA flow pattern occurs at P/h=0.6; the SLR flow pattern occurs at P/h=1.0-3.0; the VWA flow pattern occurs at P/h=3.5-3.6 and the VI flow pattern occurs at P/h=3.7-4.0.

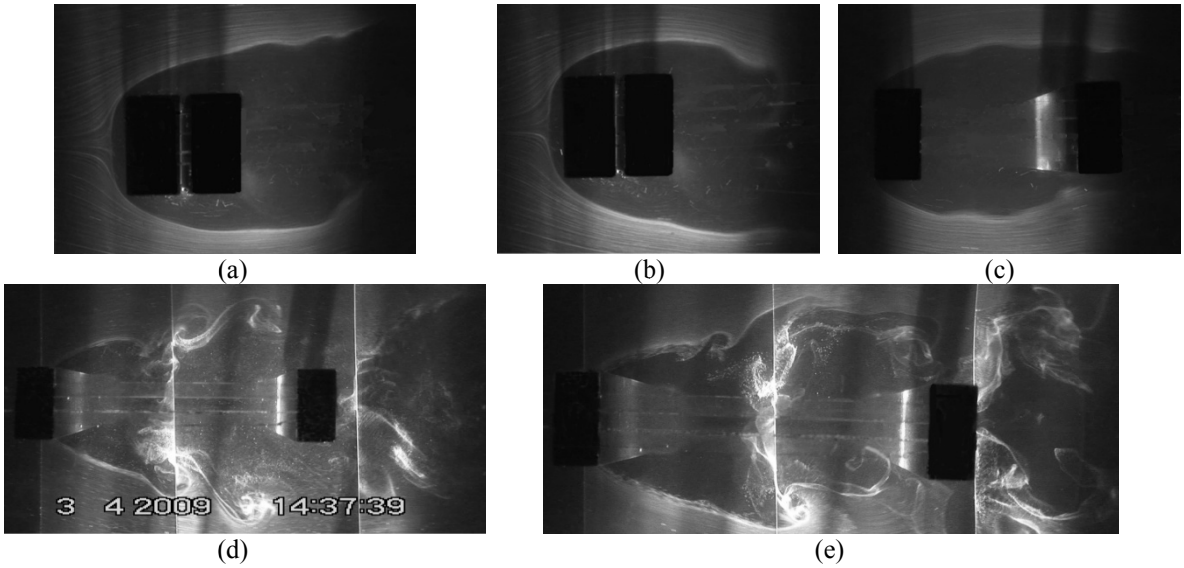

Fig. 4 Flow visualizations at: (a)-(b), P/h=0.6, (c), P/h=2.0, (d) P/h=3.6 and (e) P/h=4.0

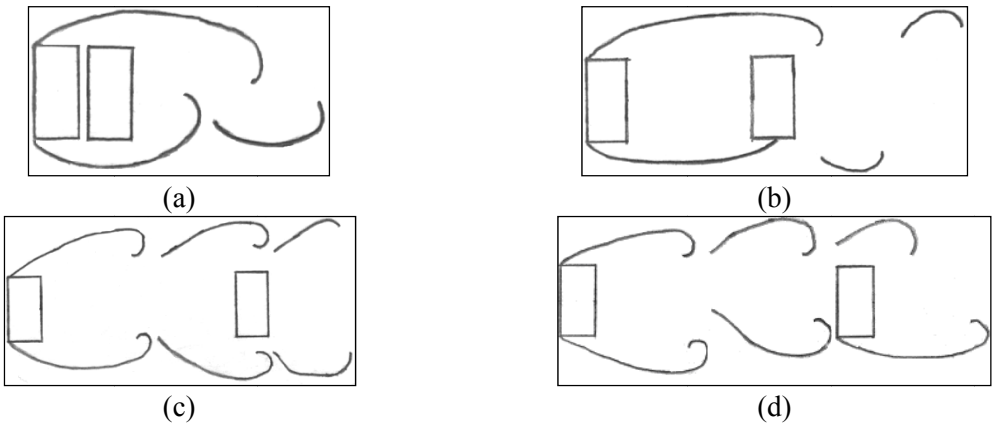

Fig. 5 Schematic representations of different flow patterns: (a) SLWA flow pattern, (b) SLR flow pattern, (c) VWA flow pattern and (d) VI flow pattern

At P/h=0.6 of the SLWA flow pattern, only one St=0.111, which is smaller than that of the isolated cylinder, is detected on the two cylinders. This is due to the fact that in this configuration, the two cylinders behave like one 'rectangular cylinder' with 'b/h' about 1.0, causing the St is lower than that of the isolated one, which is agreed with Nakaguchi *et al*. (1968). However, the strength of the peak, as shown in Fig. 6(a), is almost the same with that on the isolated one. Further more, 2St=0.222 are detected on the taps u9 and d5, as shown in Fig. 6(a), attributing to the alternate shedding of the shear layers, which are shown in Figs. 4(a) and (b) of §3.3.

For the SLR flow pattern, at P/h=1.0-2.5, one St about 0.137, which is larger than that of the

isolated one, is detected on the two cylinders. Since the gap region is still 'stagnant', as mentioned in §3.2, the large St may be attributing to the 'one-body' effect with a large aspect ratio. This result is similar with that observed by Okajima (1982), Norberg (1993) and Sohankar (2008), where a large St was detected on a rectangular cylinder with aspect ratio of 3.0. Meanwhile, 2St detected on d5 and d9 are due to the fact that the shear layer from the upstream cylinder alternately attaches onto the side of the downstream cylinder. On the other hand, from Figs. 6(b) and (c) it can be seen that the strength of the peak on the upstream cylinder is getting smaller with the increase of P/h. Further more, compared Fig. 6(c) with Fig. 7(a), it is evident that the strength of the peak on the downstream cylinder is higher than that on the upstream cylinder. The reason is that the vortices rolled up by the separated shear layers move further from the upstream cylinder and are formed behind the downstream cylinder. A special state occurs at P/h=3.0, when no peak is detected on the upstream cylinder (as shown in Fig. 6(d)) as well as a distinct peak is detected on the downstream cylinder (as shown in Fig. 7(b)). Meanwhile, compared with P/h=1.0-2.5, the peak near a smaller St=0.123 is detected on the downstream cylinder, meaning that the 'one-body' effect is suppressed.

For the VWA flow pattern at P/h=3.5-3.6, one St, which decreases rapidly to about 0.108, is detected on the two cylinders. This is due to the fact that the existence of the downstream cylinder will decrease the frequency of the vortex shedding from the upstream cylinder. Meanwhile, compared Fig. 6(e) with Fig. 7(c), the strength of the vortex detected on the upstream cylinder is much lower than that on the downstream cylinder, which is similar with the SLR flow pattern.

For the VI flow pattern at P/h=3.7-4.0, one St about 0.105 is detected on the two cylinders, which is slightly smaller than that at the VWA flow pattern. This is due to the fact that in this pattern the suppression effect of the downstream cylinder is more evident, as shown in Fig. 4(e). From the flow visualizations video, it is believed that the vortices shedding from the downstream cylinder are triggered by the arrival vortices of the upstream cylinder, which was also observed by Sakamoto and Haniu (1988), in the case of the tandem arrangement at S/W>3.5 and Sumner *et al*. (2005) at the widely spaced staggered configurations at α=0°, P/D=4.0. The difference of the pitch ratio is caused by the different experimental conditions.

Table1 Variations of Strouhal numbers with P/h

Taps \ P/h	0.6	1.0	1.5	2.0	2.5	3.0	3.5	3.6	3.7	4.0
u7	0.111	0.137	0.137	0.138	0.137	—	0.107	0.108	0.106	0.105
u9	0.111/ 0.222	0.137	0.137	0.138	0.137	—	0.107	0.108	0.106	0.105
d5	0.111/ 0.222	0.137/ 0.274	0.137/ 0.274	0.138/ 0.276	0.137/ 0.274	0.123	0.107	0.108	0.106	0.105
d7	0.111	0.137	0.137	0.138	0.137	0.123	0.107	0.108	0.106	0.105
d9	0.111	0.137/ 0.274	0.137/ 0.274	0.138/ 0.276	0.137/ 0.274	0.123	0.107	0.108	0.106	0.105

Note: '—'denoting no peak detected.

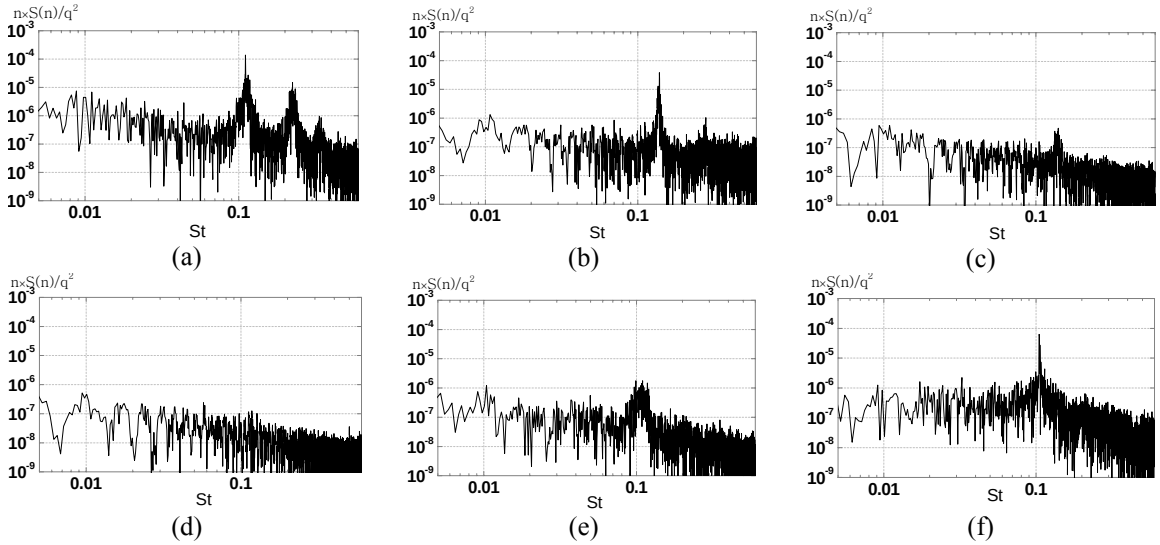

Fig. 6 Power spectral density on u9 at P/h: (a) 0.6, (b) 1.0, (c) 2.0, (d) 3.0, (e) 3.6 and (f) 4.0.

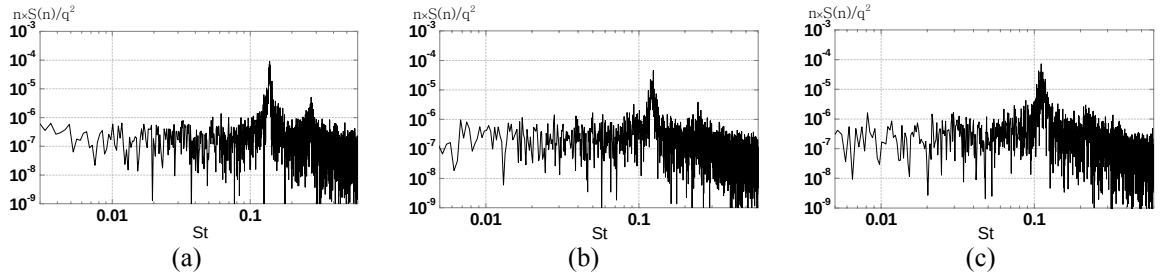

Fig. 7 Power spectral density on d9 at P/h: (a) 2.0, (b) 3.0 and (c) 3.6

4. Conclusions

In this study, flow patterns around two rectangular cylinders in tandem arrangement were investigated by the pressure measurements and the flow visualizations under the uniform smooth flow conditions. Pitch ratio P/h ranged from 0.6 to 4.0. Four distinct flow patterns with their interactions of the shear layers and vortices around the two cylinders are identified. The characteristics of the Strouhal numbers on each flow pattern are discussed. The pitch ratio boundaries for the flow patterns are also proposed, limited to the experimental test.

In the SLWA flow pattern with small P/h=0.6, the shear layers from the upstream cylinder wrap around and enclose the downstream cylinder. The two cylinders behave like ‘one body’ with aspect ratio about 1.0, resulting in a smaller St than that of the isolated one. Meanwhile, the mean and rms pressure distributions on the side and back surfaces of the downstream cylinder are quite similar with that of the isolated one.

In the SLR flow pattern with P/h=1.0-3.0, the shear layers separated from the upstream cylinder

alternately reattach onto the side surfaces of the downstream cylinder with enclosing the gap region. The two cylinders behave like 'one body' with a large aspect ratio, resulting in a larger St than that of the isolated cylinder. On the other hand, the C_{ps} of the downstream cylinder indicate that a reattachment occurs. Compared with the SLWA flow pattern, the shedding strength of the shear layers is weaker, resulting in the smaller C_{rms} on the two cylinders.

In the VWA flow pattern with P/h=3.5-3.6, the vortices shedding from the two sides of the upstream cylinder warp around the downstream cylinder, resulting in a small St. This is due to the significant suppression effect of the downstream cylinder. No reattachment occurs on the side of the downstream cylinder again. Compared with the SLR flow pattern, the C_{rms} on the two cylinders, especially on the front surface of the downstream cylinder, are larger.

In the VI flow pattern with P/h=3.7-4.0, the vortices shedding from the side surfaces of the upstream cylinder impinge upon the front surface of the downstream cylinder alternately, resulting in the smallest St, which is due to the most evident suppression effect of the downstream cylinder. Meanwhile, the 'impingement' results in an abrupt increase of C_p and C_{rms} on the front surface of the downstream cylinder, and a 'jump' of C_D.

References

Bailey, P.A. (1985), "Interference excitation of twin buildings", *J. Wind Eng, Ind. Aerod.*, **21**(3), 323-338.

Courchesne, J. and Laneville, A. (1979), "A Comparison of correction methods used on the evaluation of drag coefficient measurement for two-dimensional rectangular cylinders", *J. Fluid. Eng.- T. ASME*, **101**, 506-510.

Hu, J.C. and Zhou, Y. (2008), "Flow structure behind two staggered circular cylinders. Part 1. Downstream evolution and classification", *J. Fluid Mech.*, **607**, 51-80.

Kim, M.K., Kim, D.K., Yoon, S.H. and Lee, D.H. (2008), "Measurements of the flow fields around two square cylinders in a tandem arrangement", *J. Mech.Sci.Technol.*, **22**(2), 2397-2407

Laneville, A. and Lu, A.Y. (1983), "Mean flow patterns around 2-D rectangular cylinders and their interpretation", *J. Wind Eng. Ind. Aerod.*, **14**(1-3), 387-398.

Lim, H.C. (2009), "Wind flow around rectangular obstacles with aspect ratio", *Wind Struct.*, **12**(4), 299-312.

Liu, C.H. and Chen, J.M. (2002), "Observations of hysteresisi in flow around two square cylinders in a tandem arrangement", *J. Wind Eng. Ind. Aerod.*, **90**(9), 1019-1050.

Luo, S.C. and Teng, T.C. (1990), "Aerodynamic forces on a square section cylinder that is downstream to an identical cylinder", *J. Aeronaut.*, **94**(936), 203-212.

Luo, S.C., Li, L.L. and Shah, D.A. (1999), "Aerodynamic stability of the downstream of two tandem square-section cylinders", *J. Wind Eng. Ind. Aerod.*, **79**(1-2), 79-103.

Nakaguchi, H., Hashimoto, K. and Muto, S. (1968), "An experimental study on aerodynamic drag of rectangular cylinder", *J. Japen Soc. Aeromaut. Space Sci., (in Japanese)*, **16**, 1-5.

Noda, H. and Nakayama, N. (2003), "Free-stream turbulence effects on the instantaneous pressure and forces on cylinders of rectangular cross section", *Exper. Fluid.*, **34**(3), 332-344.

Norberg, C. (1993), "Flow around rectangular cylinders, pressure forces and wake frequencies", *J. Wind Eng.Ind. Aerod.*, **49**(1-3), 187-196.

Okajima, S. (1982), "Strouhal numbers of rectangular cylinder", *J. Fluid Mech.*, **123**, 379-398.

Oka, S. and Ishihara, T. (2009), "Numerical study of aerodynamic characteristics of a square prism in a uniform flow", *J. Wind Eng. Ind. Aerod.*, **97**(11-12), 548-559.

Sakamoto, H., Haniu, H. and Obata, Y. (1987), "Fluctuating forces acting on two square prisms in a tandem arrangement", *J. Wind Eng. Ind. Aerod.*, **26**(1), 85-103.

Sakamoto, H. and Haniu, H. (1988), "Aerodynamic forces acting on two square prisms placed vertically in a turbulent boundary layer", *J. Wind Eng. Ind. Aerod.*, **31**(1), 41-66.

Sohankar, A. (2008), "Large eddy simulation of flow past rectangular-section cylinders: Side ratio effects", *J. Wind Eng. Ind. Aerod.*, **96**(5), 640-655.
Sumner, D., Price, S.J. and Paidoussis, M.P. (2000), "Flow-pattern identification for two staggered circular cylinders in cross-flow", *J. Fluid Mech.*, **411**, 263-303.
Sumner, D., Richards, M.D. and Akosile, O.O. (2005), "Two staggered circular cylinders of equal diameter in cross-flow", *J. Fluid. Struct*., **20**(2), 255-276.
Sun, T.F. and Gu, Z.F. (1995), "Interference between wind loading on group of structure", *J. Wind Eng. Ind. Aerod.*, **54-55**, 213-225.
Xie, Z. and Gu, M. (2005), "Wind-induced interference effects between two arbitrarily arranged prisms", *China Civil Eng. J.. (in Chinese)*, **38**, 32-38.
Yu, D.H. and Kareem, A. (1997), "Numerical simulation of flow past rectangular-section cylinders: Side ratio effects", *J. Wind Eng.Ind. Aerod.*, **67-68**, 195-208.
Zhang, A. and Gu, M. (2008), "Wind tunnel tests and numerical simulations of wind pressures on buildings in staggered arrangement", *J. Wind Eng. Ind. Aerod.*, **96**(10-11), 2067-2079.